Article

Phase Optimization for Multipoint Haptic Feedback Based on Ultrasound Array

Zhili Long [1], Shuyuan Ye [1], Zhao Peng[1], Yuyang Yuan[1] and Zuohua Li*

[1] Harbin Institute of Technology Shenzhen, Shenzhen 518055, China; longzhili@hit.edu.cn(Z.L.); 2111683050@qq.com(S.Y.); 731342693@qq.com(Z.P.); 3179077768@qq.com(Y.Y.);
* Correspondence: lizuohua@hit.edu.cn; Tel.: +86-13420948695

Abstract: Ultrasound based haptic feedback is a potential technology for human-computer interaction (HCI) with the advantages of low cost, low power consumption and controlled force. In this paper, the phase optimization for multipoint haptic feedback based on ultrasound array is investigated and the corresponding experimental verification is provided. A mathematical model of acoustic pressure is established for the ultrasound array and then a phase optimization model for an ultrasound transducer is constructed. We propose a pseudo-inverse (PINV) algorithm to accurately determine the phase contribution of each transducer in the ultrasound array. By controlling the phase difference of the ultrasound array, the multipoint focusing forces are formed leading to various shapes such as geometries and letters that can be visualized. Because the unconstrained PINV solution results in unequal amplitudes for each transducer, a weighted amplitude iterative optimization is deployed to further optimize the phase solution, by which the uniform amplitude distributions of each transducer are obtained. For the purpose of experimental verifications, a platform of ultrasound haptic feedback consisting of a Field Programmable Gate Array (FPGA), an electrical circuit and an ultrasound transducer array is prototyped. The haptic performances of single point, multiple points and dynamic trajectory were verified by controlling the ultrasound force exerted on the liquid surface. The experimental results demonstrate that the proposed phase optimization model and theoretical results are effective and feasible, and the acoustic pressure distribution is consistent with the simulation results.

Keywords: Haptic feedback; Phase optimization; Pseudo-inverse algorithm; Ultrasound array

1. Introduction

HUMAN-COMPUTER interaction (HCI), which evolves from a general level of mouse-keyboard communication to an advanced stage of speech-gesture control, is a fundamental technology in the Internet of Things. Haptic feedback, as an essential technology of HCI, can significantly increase the sensing and perception when integrated with audio-vision communication [1]. Moreover, haptic feedback has widespread applications, such as emotional interaction, teleoperation, and medical training [2-5].

Currently, researchers and engineers specialized in haptic development mainly focus on wearable haptic devices which can provide touchable feedback [6]. Bouzit et al. designed the Master II-ND, which used custom pneumatic[]actuators arranged in a direct-drive configuration between the palm and the thumb, index middle and ring fingers [7]. The glove was connected to a haptic control interface that reads its sensors and drives its actuators. Inrak Choi et al. developed a Wolverine system, which can withstand over 100 N of force between each finger and the thumb with the power consumption as low as 0.24 mWh for each braking interaction [8]. Integrated sensors were employed for both feedback control and user input. Specifically, time-of-flight sensors were used to determine the position of each finger and an inertial measurement unit (IMU) was manipulated for the overall orientational tracking. Qin et al. designed and calibrated a new 6 DOF (degree-of-freedom) haptic device [9, 10]. It consisted of a double parallel linkage,

a rhombus linkage, a rotational mechanical structure and a grasping interface, which is capable of multifinger interactions. These tactile haptic devices have the advantages of strong feedback and high control accuracy. However, most of them are complex and cumbersome in structure. Moreover, there are unexpected haptic feelings due to the tactile sensors.

In order to overcome the shortcomings of tactile haptic feedback, some noncontact haptic feedback technologies are proposed. Suzuki et al. developed a force feedback technique based on air pressure, which would be the basis of a handy untethered human interface [11]. Gupta et al. designed the AirWave system based on an air vortex ring [12]. They showed through objective measurements that AirWave can achieve spatial resolution of less than 10 cm at a distance of 2.5 meters. They further demonstrated through a user study that this can be used to generate direct haptic stimuli to different regions of the human body. Rajinder et al. designed the AIREAL system based on a similar theory [13]. Combined with interactive computer graphics, AIREAL enables users to feel virtual 3D objects, experience free air textures, and receive haptic feedback on gestures performed in the free space. However, haptic feedback based on air pressure has some disadvantages, such as fixed direction of air injection and unsustainable pressure. Weiss et al. proposed the FingerFlux system based on electromagnet arrays [14]. FingerFlux allowed users to feel the interface before touching, and could also create both attracting and repelling forces. Studies showed that users could feel vibration patterns up to 35 mm above the table, and that FingerFlux could significantly reduce drifting when operating on-screen buttons without looking. However, the operator needed to stick a permanent magnet on the finger with limited effective sensing range. Tong et al. designed a novel magnetic levitation haptic device based on electromagnetic theory [15]. The users could directly sense virtual tissues by moving a magnetic stylus in the magnetic field generated by the coil array of their device. Yoichi et al. presented a new method of rendering aerial haptic images that uses femtosecond-laser light fields and ultrasound acoustic fields [16]. They used femtosecond lasers to create plasma in the air and scanned it at a high speed to achieve various three-dimensional effects [17]. However, the workspace of the system was limited to only 1cm3.

With distinct advantages of strong penetration, low cost, low power consumption, and controllability, haptic feedback based on ultrasound radiation has attracted more attention and interest than ever before [18]. Shinoda et al. firstly proposed the noncontact midair haptic feedback based on ultrasound transducer array. Phase control was used to focus the energy to form a stable pressure at the focal point, and the linear movement of the haptic feedback point was implemented by controlling the position change of the focal point [19,20]. Based on this technology, they further developed many new HCI devices combining both ultrasound haptic feedback and visual system [21-25]. Gavrilov et al. proposed the concept of control points to solve the multipoint focusing problem [26]. It was shown that the arrays make it possible to form the regions of action by focused ultrasound with various necessary shapes and the sidelobe (or other secondary peak) intensity level acceptable for practical purposes. Using these arrays, it was possible to move the set of foci off the array axis to a distance of at least ±5 mm. In the framework of Gavrilov's research, Tom Carter et al. implemented multipoint focusing based on the ultrasound array [27]. They invented an Ultrahaptics system to demonstrate a spatial and multipoint haptic feedback interaction. Through psychophysical experiments they showed that feedback points with different haptic properties could be identified at smaller separations. They also showed that users could distinguish between different vibration frequencies of noncontact points with training. Long B. et al. analyzed the characteristic roots of the phase matrix and used the Weighted Tikhonov Regularization method to optimize the phase in order to reduce the power loss caused by the introduction of frequency modulation for haptic sensation [28]. With these, they then implemented the focus point distribution in various shapes. Georgios et al. developed the Haptogram system with high-frequency switching which was designed to provide point-cloud haptic display via acoustic radiation pressure [29]. A tiled 2-D array of ul-

Preprints (www.preprints.org) | NOT PEER-REVIEWED | Posted: 27 December 2021 doi:10.20944/preprints202112.0434.v1

trasound transducers was used to produce a focal point that was animated to produce arbitrary 2-D and 3-D haptic shapes.

The noncontact haptic feedback with many competitive advantages is an inevitable trend for the future of HCI. Noncontact haptic feedback based on the air vortex ring and electromagnetics have the shortcomings of limited effective range and inconvenient control. In contrast, ultrasound arrays are more flexible due to the controlled phase and have a much larger effective range. Currently, researchers majoring in ultrasound haptic feedback are concentrating on the single-point focusing, and existing discussions for multipoint focusing are rare at best. Actually, how to attain the phase difference of each ultrasound transducer is fundamental to generate various focus points, especially when the ultrasound arrays are in a large number. Moreover, generating multiple forces will be impossible without a sufficiently accurate calculation model. In this study, we propose an effective optimization approach for the phase calculation in the multipoint haptic feedback, which is verified by experiments.

The paper is organized as follows: Section II establishes the mathematical model of the acoustic radiation force for ultrasound array and introduces the phase control for single-point focusing. The phase optimization model for multipoint haptic feedback is proposed in Section III. In Section IV, the phase optimization is verified through single-point and multipoint haptic feedback experiments using our self-developed ultrasound platform. Section V draws the conclusion.

2. Acoustic radiation force model

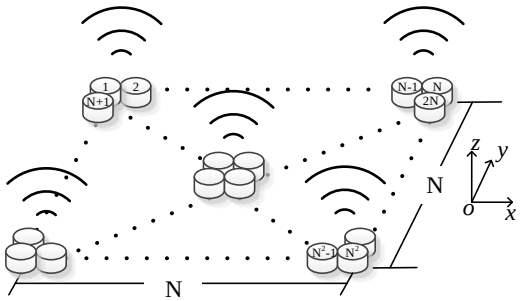

Figure 1. $N \times N$ ultrasound transducer array.

An ultrasound transducer can emit continual mechanical vibrations in high frequency, when it is driven by a voltage. We set the ultrasound array as N rows and N columns, denoted by N×N, in our design as shown in Fig. 1.

As to the i-th ultrasound transducer, its ultrasound radiation pressure pi under the polar coordinates r (the radial coordinate) and θ (the angular coordinate, often called the polar angle) is expressed as **Error! Reference source not found.**,

$$p_i(r,\theta,t) = j\frac{\rho_0 u_0 a^2 \omega}{2r}\cdot\frac{2J_1(ka\sin\theta)}{ka\sin\theta}\cdot e^{j(\omega t-kr)} \tag{1}$$

where a is the transducer radius, ϱ0 is the median (air) density, u0 is the acoustic amplitude constant, ω=2πf in which f=40 kHz is the ultrasound frequency, $k=\omega/c_0$ is the wave numbers where c0 is the ultrasound velocity in the air, and J1(∗) represents the first-order Bessel function.

The total ultrasound pressure at the location of r and θ in the N×N array is a linear superposition of the pressure of each transducer as below,

$$P(r,\theta,t)=\sum_{i=1}^{N^2} p_i(r,\theta,t) \tag{2}$$

The root mean square (RMS) value of the ultrasound pressure is obtained over a period T,

$$P_{\text{rms}}=\sqrt{\frac{1}{T}\int_0^T P^2 dt} \tag{3}$$

Preprints (www.preprints.org) | NOT PEER-REVIEWED | Posted: 27 December 2021 doi:10.20944/preprints202112.0434.v1

By controlling the emitting phase of each transducer at different locations, the ultrasound pressure of each transducer can be focused at a certain point. The time of flight (TOF) of the ultrasound wave from the i-th transducer to the focal point is obtained as,

$$\Delta t_i = \frac{\sqrt{(x-x_i)^2+(y-y_i)^2+z^2}}{c_0} \tag{4}$$

where (x, y, z) is the location of the focal point, and (xi, yi, 0) is the location of the i-th transducer.

The phase difference Di, which signifies the delay of each transducer, is calculated as,

$$D_i = T - \mathrm{mod}\left(\Delta t_i, T\right) \tag{5}$$

where mod (*) is the mode-taking operation.

Thus, the ultrasound pressure of each transducer is determined by substituting the phase difference Di into the radiation pressure pi according to (1), and then the focal pressure is obtained by superposition of each transducer.

The simulation using MATLAB as shown in Fig. 2 demonstrates two typical calculations with single focal point, where the desirable focal point is set to be 20 cm distance over the plane of ultrasound array whereas they are at different locations as shown in Fig. 2. a). Fig. 2 b) shows the phase difference distribution of each transducer calculated by Expression (5). Fig. 2 c) shows the normalized ultrasound pressure distribution, which means that the ultrasound pressure can be focused by controlling the phase difference of each transducer.

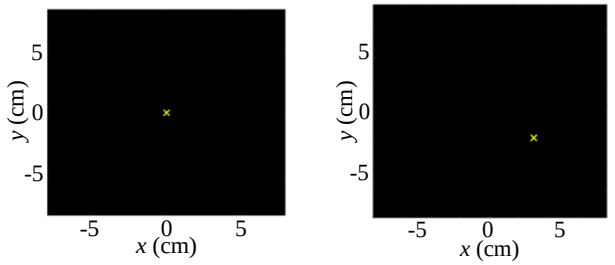

a) Desirable focal point

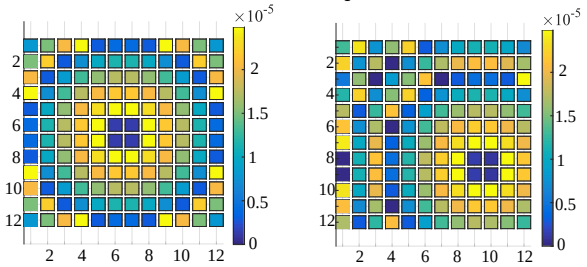

b) Phase distribution

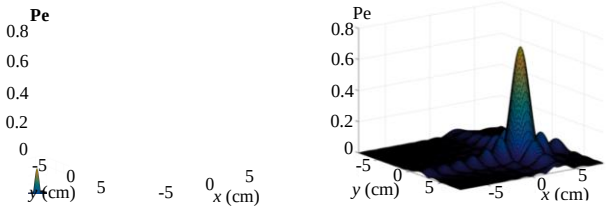

c) Ultrasound pressure distribution

Figure 2. Simulation of single focal point. a) and b) is the phase difference distribution of each transducer. c) is the normalized ultrasound pressure distribution.

3. Optimization Model For Multipoint Focusing

3.1. Optimization Model Based Pseudo-inverse (PINV)

Preprints (www.preprints.org) | NOT PEER-REVIEWED | Posted: 27 December 2021 doi:10.20944/preprints202112.0434.v1

In this section, we show that we can also control the phase difference of each transducer to generate multiple focusing points. In our study, the ultrasound transducer array is set to be 16×16. When many desirable focus points exist, it is challenging to attain the phase difference of each transducer due to the high dimensional matrix. For this, we propose the pseudo-inverse (PINV) approach to intelligently pinpoint the effective solutions.

With the phase difference Di, we can obtain the ultrasound pressure of the i-th transducer in the array, as

$$p_i(r,\theta)=\left(j\frac{\rho_0\omega a^2}{2r}\cdot\frac{2J_1(ka\sin\theta)}{ka\sin\theta}\cdot e^{j(-kr)}\right)\cdot\left(u_0e^{-j\omega D_i}\right) \tag{6}$$

which can be defined as pi=Hi·ui, where

$\boldsymbol{H}_i = j\frac{\rho_0\omega a^2}{2r}\cdot\frac{2J_1(ka\sin\theta)}{ka\sin\theta}\cdot e^{j(-kr)}$ is constant if the location and radius of the i-th transducer are determined. Note that $u_i = u_0e^{-j\omega D_i}$ contains the amplitude and phase of the i-th transducer.

The total pressure of the transducer array N×N is obtained by the following linear superposition,

$$P=\sum_{i=1}^{N^2}p_i=\sum_{i=1}^{N^2}\boldsymbol{H}_i\cdot u_i \tag{7}$$

$$P=\begin{bmatrix}\boldsymbol{H}_1 & \boldsymbol{H}_2 & \dots & \boldsymbol{H}_N\end{bmatrix}\cdot\begin{bmatrix}u_1\\u_2\\\vdots\\u_N\end{bmatrix} \tag{8}$$

That is,

Assuming that there are M desirable focal points being P1, P2, …, and PM, we can get

$$\begin{pmatrix}P_1\\\vdots\\P_M\end{pmatrix}=\begin{pmatrix}H_{11} & \dots & H_{1N}\\\vdots & \ddots & \vdots\\H_{M1} & \dots & H_{MN}\end{pmatrix}\times\begin{pmatrix}u_1\\\vdots\\u_N\end{pmatrix} \tag{9}$$

which can be simplified as,

$$PM\times1 = HM\times N\cdot uN\times1 \tag{10}$$

where HM×N represents the forward calculation of the ultrasound pressure of those M focus points and N transducers, uN×1 is a complex matrix containing the amplitudes and phases of those N transducers, and PM×1 is a matrix containing the ultrasound pressure amplitudes of those M focus points. Then, the optimization function of ultrasound pressure is determined as,

$$\min_u \; f(\boldsymbol{u})=\|\boldsymbol{Hu}-\boldsymbol{P}\|^2 \tag{11}$$

Our target is to determine the amplitude and phase u of each transducer so that the total ultrasound pressure Hu is closest to the desirable pressure distribution P.

Generally, the number of desirable focal points is less than that of the transducers, i.e., M < N2. Since the matrix H is of full rank in row, its right inverse matrix exists. By formulating the right inverse of H, the minimum norm solution of the expression (11) is equal to

$$\begin{aligned}&\min && \|\boldsymbol{u}\|_2\\&\text{subject to} && \boldsymbol{Hu}=\boldsymbol{P}\end{aligned} \tag{12}$$

The solution is,

$$\boldsymbol{u}=\boldsymbol{H}^{*T}\left(\boldsymbol{H}\boldsymbol{H}^{*T}\right)^{-1}\boldsymbol{P} \tag{13}$$

where H*T is the conjugate transpose of the matrix H.

Thus, the phase difference u of each transducer can be determined by applying the pseudo-inverse of H when multiple desirable focal points are set in the ultrasound array.

Preprints (www.preprints.org) | NOT PEER-REVIEWED | Posted: 27 December 2021 doi:10.20944/preprints202112.0434.v1

3.2. Calculations of Multipoint Focusing

By setting multiple focal points, the amplitude and phase of the transducers are obtained by calculating the optimization function (13).

The left and right columns in Fig. 3 shows the simulations when the numbers of the desirable pressure points are 2 and 4, respectively. In Fig. 3, a), b), c), and d) show the desirable points, phase difference distribution, amplitude distribution, and the RMS values of the ultrasound pressure, respectively. It can be seen that at the ultrasound pressures at the desirable feedback points are uniform, which meet with the desired multipoint focusing forces.

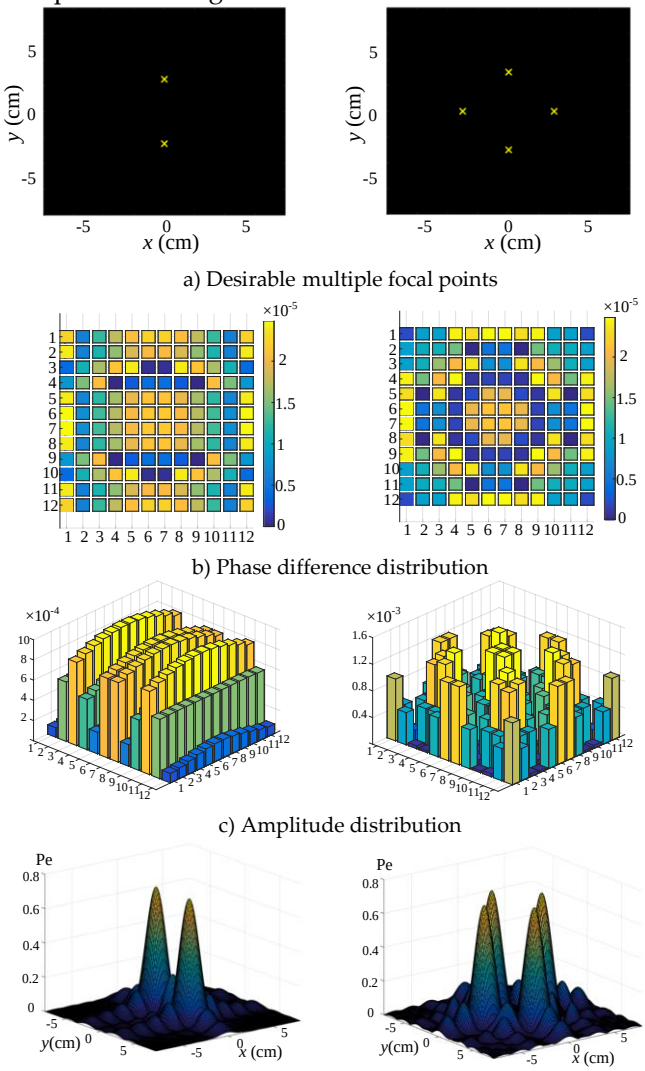

Figure 3. Simulation of multipoint focusing. a), b), c), and d) show the desirable points, phase difference distribution, amplitude distribution, and the RMS values of the ultrasound pressure, respectively.

3.3. Complex Focal Simulation

It is deduced from equation (13) that the solution by PINV calculation is not affected by the position and the number of focal points. Therefore, in order to generate haptic feedback with more complex shapes, we set more focal points and then use the PINV approach to obtain the corresponding phases. The left, middle, and right columns in Fig. 4. a) shows the desirable focal geometries arranged in the forms of circle, rectangle, and triangle, respectively. Fig. 4. b), c) and d) present the corresponding phase difference distribution, amplitude distribution, and ultrasound pressure distribution, respectively.

Preprints (www.preprints.org) | NOT PEER-REVIEWED | Posted: 27 December 2021 doi:10.20944/preprints202112.0434.v1

It can be seen that the ultrasound pressure distribution can be constructed according to the desirable geometries.

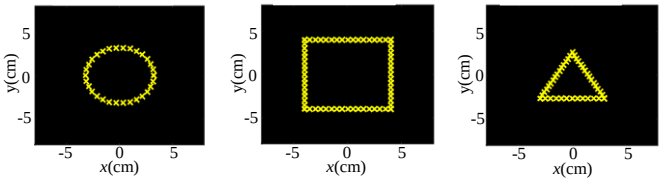

a) Desirable multiple focal geometries

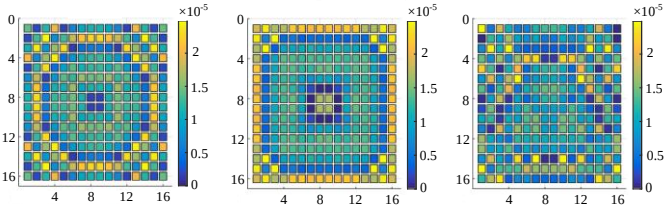

b) Phase difference distribution

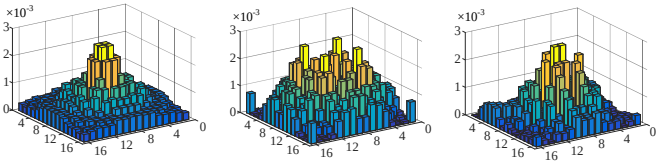

c) Amplitude distribution

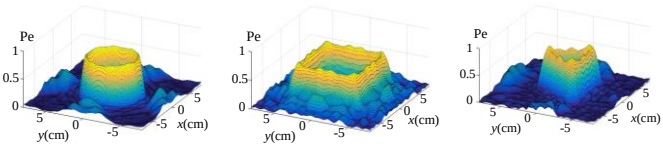

d) Ultrasound pressure distribution

Figure 4. Simulation for complex geometries. a) is the desirable focal geometries arranged in the forms of circle, rectangle, and triangle, respectively. b), c) and d) present the corresponding phase difference distribution, amplitude distribution, and ultrasound pressure distribution, respectively.

Similarly, the PINV algorithm is utilized to obtain the shapes of letters. The left, middle, and right columns in Fig. 5. a) demonstrate the desirable focal letters of H, I, and T, respectively, and the corresponding phase distribution, amplitude distribution, and ultrasound pressure distribution are demonstrated in Fig. 5 b), c), and d), respectively. Through these simulations, it is proved that the PINV can obtain a reasonable phase to form a desirable pressure distribution in the shape of certain geometries and various letters.

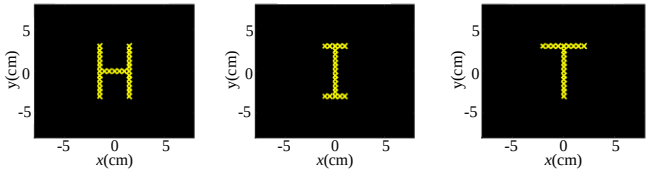

a) Desirable focus

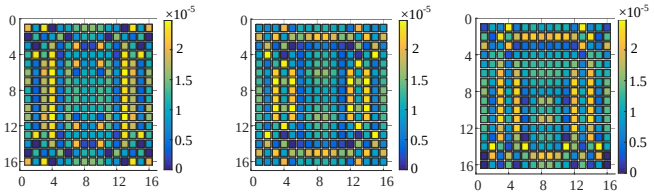

b) Phase difference distribution

Preprints (www.preprints.org) | NOT PEER-REVIEWED | Posted: 27 December 2021 doi:10.20944/preprints202112.0434.v1

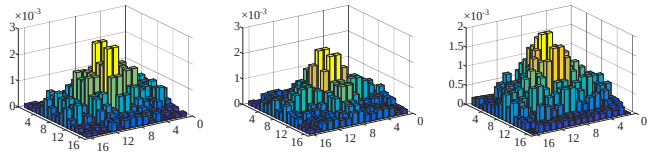

c) Amplitude distribution

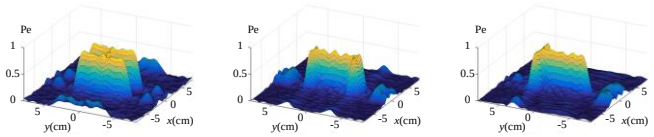

d) Ultrasound pressure distribution

Figure 5. Simulation for letters H, I and T. a) demonstrates the desirable focal letters of H, I, and T, respectively. b), c), and d) show the corresponding phase distribution, amplitude distribution, and ultrasound pressure distribution, respectively.

3.4. Uniform Amplitude Optimization

In the objective optimization based on the PINV approach, since no constraint is on the variable u, the controlled amplitudes for various transducers are different, as shown in Fig. 3 c), or Fig. 4 c), or Fig. 5 c), although the phase differences are attained. Actually, it is difficult for the electrical control module to trigger multiple transducers under different voltage amplitudes. Therefore, it is necessary to further optimize the variable u. The optimization target is to find out the phase of each transducer with uniform amplitude to satisfy Hu = P.

We propose the weighted iterative optimization algorithm to achieve the uniform amplitude of each transducer. The weighting matrix W is expressed as,

$$\boldsymbol{u}_w = \boldsymbol{W}\boldsymbol{H}^{*T}\left(\boldsymbol{H}\boldsymbol{W}\boldsymbol{H}^{*T}\right)^{-1}\boldsymbol{P} \tag{14}$$

where W is an N × N real positive definite matrix, which can be optimized by the following iterative procedure, as in Table I.

TABLE I

WEIGHTED ITERATIVE OPTIMIZATION ALGORITHM

Step 0: Initialize $\boldsymbol{W} = \boldsymbol{I}$, $\boldsymbol{I}$ is the identity matrix.

Step 1: compute $\boldsymbol{u}_w$ and η by the following expression,

$$\boldsymbol{u}_W = \boldsymbol{W}\boldsymbol{H}^{*T}\left(\boldsymbol{H}\boldsymbol{W}\boldsymbol{H}^{*T}\right)^{-1}\boldsymbol{P}$$

$$\eta = \frac{\sum_{i=1}^{N^2}|\boldsymbol{u}_i|^2}{N^2 U_{\max}^2}\times 100\%$$

If η is sufficient, then go to Step 3.

Otherwise, update $\boldsymbol{H}^{*T}$ as,

$$\boldsymbol{H}^{*T}=\boldsymbol{W}\boldsymbol{H}^{*T}$$

Step 2: Evaluate the updated the weighting matrix $\boldsymbol{W}$,

$$\boldsymbol{W}(m,n) = \begin{cases} \dfrac{1}{|u_{wn}|} & \text{for } m = n; \\ 0 & \text{otherwise;} \end{cases}$$

Go to step 1.

where $\{u_{wn}, n = 1, 2, \ldots, N^2\}$ contains the elements of the vector u_w.

Step 3: The excitation vector $\boldsymbol{u} = \boldsymbol{u}_w$.

The process of the uniform amplitude optimization for five-points focusing is demonstrated in Fig. 6. a) shows the amplitudes without optimization. The amplitudes with 1, 3, and 7 iterations of the weighted optimization are shown in Fig. 6. b), c), and d) respectively. It is shown that the amplitude of each transducer becomes increasingly uniform after several iterations.

Preprints (www.preprints.org) | NOT PEER-REVIEWED | Posted: 27 December 2021 doi:10.20944/preprints202112.0434.v1

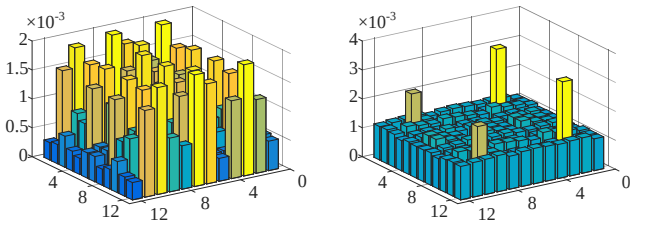

a) Amplitude with 0 iteration (without optimization)

b) Amplitude with 1 iteration

c) Amplitude with 3 iterations

d) Amplitude with 7 iterations

Figure 6. Iterative optimization for uniform amplitude.

The ultrasound pressure distribution without and with optimization are presented in Fig. 7 a) and Fig. 7 b), respectively. In Fig. 7 b), although some noises are amplified, they are much smaller in magnitude than the pressure of the focal points. The ultrasound pressure amplitudes of the five focus points are nearly uniform, which is acceptable in the practical control.

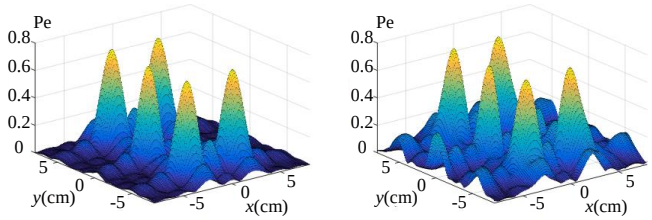

a) Without optimization

b) With optimization

Figure 7. Ultrasound pressure distributions without and with optimization.

Similarly, the weighted iterative algorithm is employed to optimize the amplitudes of circular, rectangular, and triangular shapes. In Fig. 8, the first row shows the ultrasound pressure distribution without optimization and the second row shows the result with optimization. It is obvious that although some noises appear near the desirable shapes, they are acceptable since the pressure profiles are in the same level.

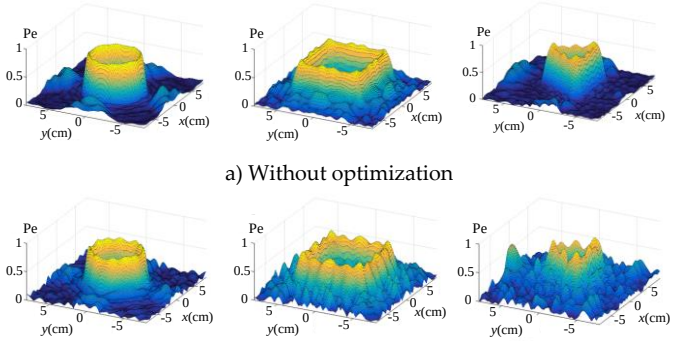

a) Without optimization

Figure 8. Pressure amplitude comparison with and without optimization. a) is the ultrasound pressure distribution without optimization and b) is the result with optimization.

Preprints (www.preprints.org) | NOT PEER-REVIEWED | Posted: 27 December 2021 doi:10.20944/preprints202112.0434.v1

4. Experiment

4.1. Experimental Platform

In order to verify the feasibility of the proposed phase optimization approach, we deploy the haptic feedback experiments including single-point, multipoint and dynamic trajectory verifications. Figure 9 a) shows the implementation procedure for the ultrasound haptic feedback from simulations to experiments. Firstly, the desirable shape is determined and then imported into the PINV optimizer to obtain the initial phase. Then, the weighted iterative optimization presented in Section III is carried out to achieve the uniform amplitude. Meantime, the phase is updated and then downloaded into the FPGA controller, which triggers the ultrasound array using the optimized phases.
Figure 9 b) shows the hardware architecture of the ultrasound control system. It consists of an ultrasound transducer array, an FPGA controller, a power amplification module, a computer, and an acoustic measurement system. The ultrasonic array consists of 16×16 ultrasonic transducers arranged in the shape of a square. Each transducer has a high frequency of 40 kHz and the emission angles are within ±30 degrees. The FPGA model XC6SLX9 is selected as the controller. The IX4427 chip is chosen to amplify the FPGA signal to 15V. The transducer arrays are triggered in a certain phase sequence, as shown in Fig. 9 c). Finally, the ultrasound pressures are focused on the liquid surface in order to visualize the actual distribution of the ultrasound force. The distance between the ultrasound array and the liquid surface is 10 cm. The frequency modulation ranging from 40 to 300 Hz for each PWM signal is implemented to successfully generate the haptic stimulus sensing [31].

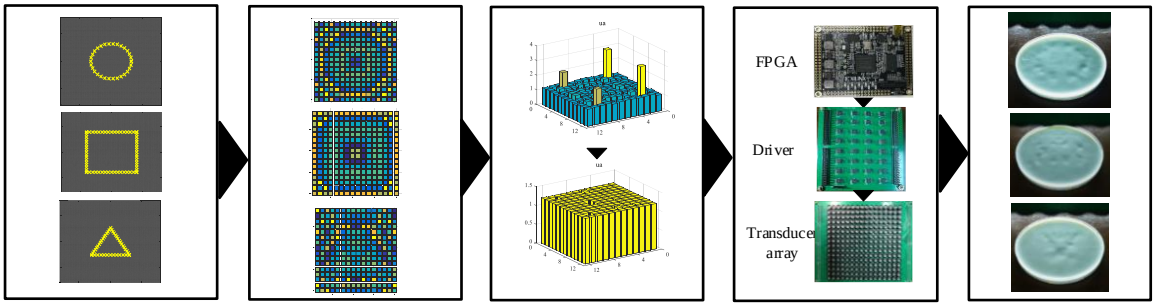

a) Implementation procedure

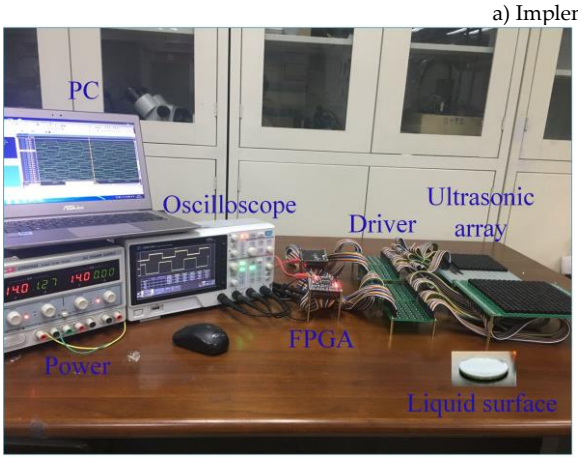

b) Hardware architecture

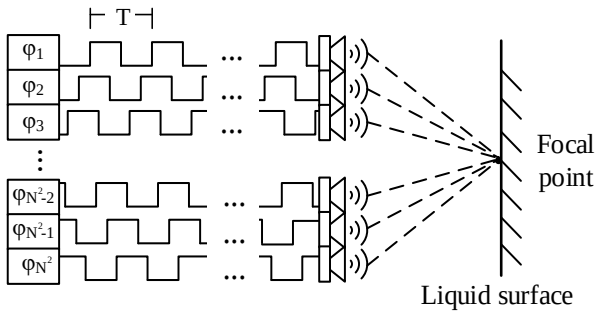

c) Ultrasound focus by array control

Figure 9. Experimental platform. a) is the implementation procedure for the ultrasound haptic feedback from simulations to experiments. b) shows the hardware architecture of the ultrasound control system. c) shows that the transducer arrays are triggered in a certain phase sequence.

Preprints (www.preprints.org) | NOT PEER-REVIEWED | Posted: 27 December 2021 doi:10.20944/preprints202112.0434.v1

4.2. Single Point Haptic Feedback

Figure 10 a) shows the liquid surface under the ultrasound pressure of a single point. We can observe that an obvious distortion exists on the liquid surface, meaning that the ultrasound force emitted by the transducer array is successfully focused with strong radiation pressure. Then, we put the palm over the transducer array to feel the haptic sensing, as shown in Fig.10 b). When the palm moves downward, we can feel the force from haptic feedback at the center of the palm, and the touch feeling is that an air column is blowing toward the palm.

a) Liquid surface of single point focus

b) Haptic sensing to the palm

Figure 10. Single point haptic feedback.

The location of the single point haptic sensing can be dynamically modified, if the controlled phases of the transducer array are in an appropriate combination. We switch the controlled phase of the ultrasound transducers continuously to achieve dynamic trajectory feedback, which generate various movement trajectories that are upward, downward, leftward, rightward, circular, square, and triangular. Figure 11 demonstrates that the ultrasound focal force is controlled to dynamically move in a square trajectory on the liquid surface.

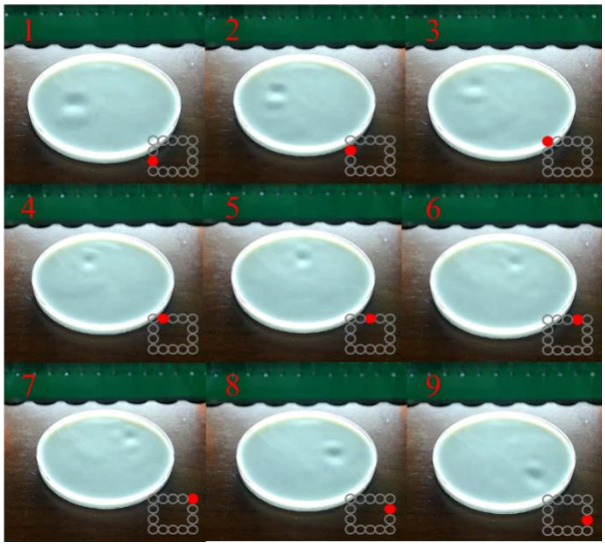

Figure 11. Dynamic movement of the ultrasound focal force.

4.3. Multipoint Haptic Feedback

Figure 12 a) and b) show the two and three desirable focal points, respectively. Figure 12 c) and d) present the depression effects on the liquid surface for the experimental verifications corresponding to Fig. a) and b), respectively. We can also find that there appear two and three depressions on the liquid surface, proving that the ultrasound pressure produced by the transducer array is consistent with the desired distribution. Figure 13 demonstrates the ultrasound pressure distribution on the liquid surface with four geometric shapes, i.e., line, circle, rectangle, and triangle. It is verified that the depression distribution on the liquid surface matches well with the locations of the desira-

Preprints (www.preprints.org) | NOT PEER-REVIEWED | Posted: 27 December 2021 doi:10.20944/preprints202112.0434.v1

ble focal points, indicating the validity of the phase solutions obtained by the optimization model.

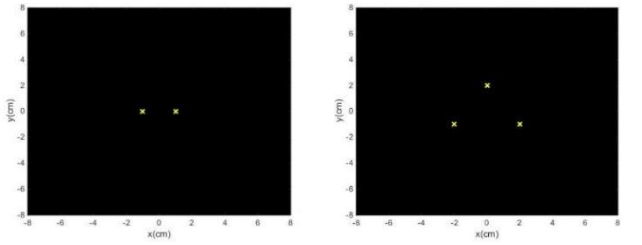

a) Desirable two-point focuses

b) Desirable three-point focuses

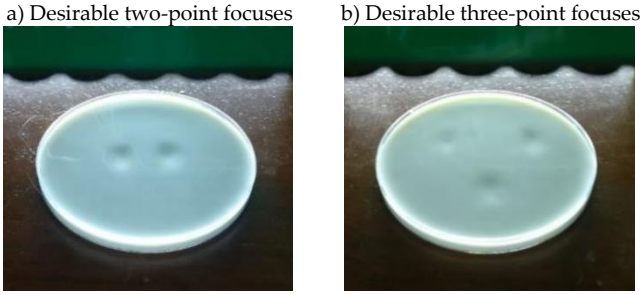

c) Two-point pressure distribution

d) Three-point pressure distribution

Figure 12. Ultrasound pressure with multiple points on liquid surface.

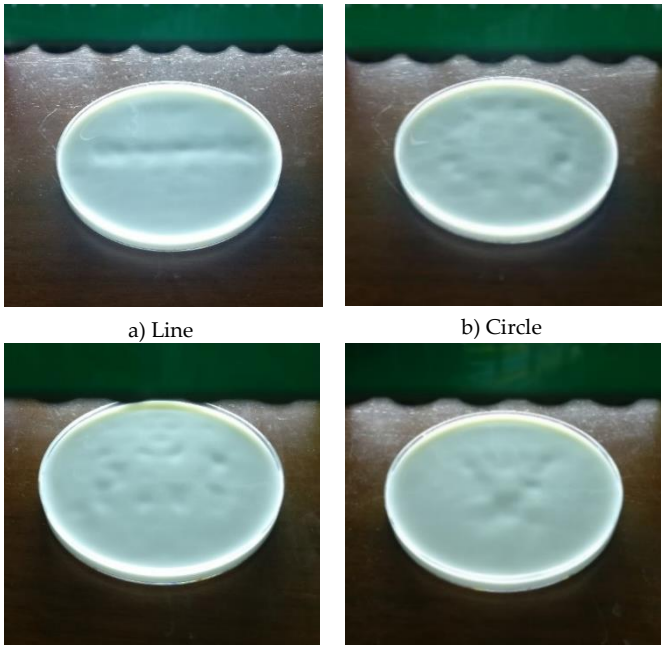

a) Line

b) Circle

c) Rectangle

d) Triangle

Figure 13. Ultrasound pressure with geometric shapes on liquid surface.

5. CONCLUSION

1) To achieve the ultrasound-based noncontact haptic feedback, we investigate the relationship between the emission force and the controlled phase of each transducer in the ultrasound phase array. By the superposition of ultrasound radiation force by appropriate phase combination, we have successfully achieved the haptic feedback of complex shapes such as circle, square, triangle, and letters. The novel technology has great potential to apply to the haptic perception and HCI due to the advantages of low price and low power consumption.

2) The mathematical model of the radiation pressure of the ultrasound array is deduced. The optimization function to intelligently searching the optimal phase is established, and the PINV algorithm is introduced to effectively solve the control phase issue. To address the inconsistent amplitudes in the PINV solutions, a weighted iterative optimization approach is proposed to further enhance the amplitude of the ultrasound array, making the electrical driving module trigger the transducer array in a uniform voltage. With these, we have carried out the simulation to visualize the multipoint haptic feedback of complex shapes such as circle, rectangle, triangle, and letter.

3) In experiment, we build up the control and driving system based on an FPGA controller. The ultrasound focal force on the liquid surface is tested. Experimental verification of the single and multipoint, and square dynamic trajectory are conducted to visualize the corresponding ultrasound pressures and focusing distributions. Experimental results prove that the proposed phase optimization and the electrical control system are feasible for the ultrasound-based haptic feedback.

In the future research, we would like to investigate various aspects of the ultrasound-based haptic feedback, including but not limited to quantification measurement of the acoustic pressure at different angles and distances, irregular amplitude control to array transducers, and tactile stimulation to human body.

Author Contributions: conceptualization, methodology and writing—review and editing, Zhili Long; software, hardware, Shuyuan Ye; original draft preparation, Zhao Peng; formal analysis, investigation, resources and data curation, Yuyang Yuan; project administration and funding acquisition, Zuohua Li.

Funding: This work was supported by the following funds: 1) National Natural Science Foundation of China (U1713206), 2) Basic Research Plan of Shenzhen (JCYJ20170413112645981, JCYJ20150928162432701), and 3) Shenzhen Technology Innovation Program (JCYJ20170811160003571).

Conflicts of Interest: The authors declare no conflict of interest.

References

1. Truong, X.; Ngo, T.D. Toward Socially Aware Robot Navigation in Dynamic and Crowded Environments: A Proactive Social Motion Model. *IEEE Transactions on Automation Science & Engineering* **2017**, 14, 1743-1760.
2. E. Maggioni, E. Agostinelli, and M. Obrist, "Measuring the added value of haptic feedback," in 2017 Ninth International Conference on Quality of Multimedia Experience (QoMEX), Erfurt, Germany, 2017, pp. 1-6.
3. E. Gatti et al., "Can the feel of the haptic interaction modify a user's emotional state? ," in 2013 World Haptics Conference (WHC), Daejeon, South Korea, 2013, pp. 247-252.
4. C. Neupert et al., "Pseudo-Haptic Feedback in Teleoperation," IEEE Transactions on Haptics, vol. 9, no. 3, pp. 397-408, Jul.-Sep. 2016.
5. T. R. Coles, D. Meglan, and N. W. John, "The Role of Haptics in Medical Training Simulators: A Survey of the State of the Art," IEEE Transactions on Haptics, vol. 4, no. 1, pp. 51-66, Jan.-Mar. 2011.
6. G. Karafotias et al., "Mid-Air Tactile Stimulation for Pain Distraction," IEEE Transactions on Haptics, vol. 11, no. 2, pp. 185-191, Apr.-Jun. 2018.
7. C. Pacchierotti et al., "Wearable Haptic Systems for the Fingertip and the Hand: Taxonomy, Review, and Perspectives," IEEE Transactions on Haptics, vol. 10, no. 4, pp. 580-600, Oct.-Dec.2017.
8. M. Bouzit et al., "The Rutgers Master II-new design force-feedback glove," IEEE/ASME Transactions on Mechatronics, vol. 7, no. 2, pp. 256-263, Jun. 2002.
9. I. Choi et al., "Wolverine: A wearable haptic interface for grasping in virtual reality," in 2016 IEEE/RSJ International Conference on Intelligent Robots and Systems (IROS), Daejeon, South Korea, 2016, pp. 986-993.
10. H. Qin, A. Song, Y. Liu, et al., "Design and Calibration of a New 6 DOF Haptic Device," Sensors, vol. 15, no. 12, pp. 31293-31313, Dec.2015.
11. H. Qin, A. Song, Z. Gao, et al., "A Multi-Finger Interface with MR Actuators for Haptic Applications," IEEE Transactions on Haptics, vol. 11, no. 1, pp. 5-14, Jan.-Mar. 2018.
12. Y. Suzuki and M. Kobayashi, "Air jet driven force feedback in virtual reality," IEEE Computer Graphics and Applications, vol. 25, no. 1, pp. 44-47, Jan.-Feb. 2005.

13. S. Gupta et al., "AirWave: Non-Contact Haptic Feedback Using Air Vortex Rings," in 2013 ACM International Joint Conference on Pervasive and Ubiquitous Computing, Zurich, Switzerland, 2013, pp. 419-428.
14. R. Sodhi et al., "AIREAL: Interactive Haptic Experiences in Free Air," ACM Transactions on Graphics, vol. 32, no. 4, pp. 1-10, Jul. 2013.
15. M. Weiss et al., "FingerFlux: Near-Surface Haptic Feedback on Tabletops," in Proceedings of the 24th Annual ACM Symposium on User Interface Software and Technology, Santa Barbara, CA, USA, 2011, pp. 615-620.
16. Q. Tong et al., "Magnetic Levitation Haptic Augmentation for Virtual Tissue Stiffness Perception," IEEE Transactions on Visualization and Computer Graphics, vol. 24, no. 12, pp. 3123-3136, Dec.2018.
17. Y. Ochiai et al., "Cross-Field Aerial Haptics: Rendering Haptic Feedback in Air with Light and Acoustic Fields," in 34th Annual CHI Conference on Human Factors in Computing Systems (CHI4GOOD), San Jose, CA, USA, 2016, pp. 3238-3247.
18. Y. Ochiai et al., " Fairy Lights in Femtoseconds: Aerial and Volumetric Graphics Rendered by Focused Femtosecond Laser Combined with Computational Holographic Fields," ACM Transactions on Graphics, to be published. DOI: 10.1145/2850414.
19. F. Arafsha et al., "Contactless haptic feedback: state of the art," in 2015 IEEE International Symposium on Haptic, Audio and Visual Environments and Games (HAVE), Ottawa, ON, Canada, 2015, pp. 24-29.
20. T. Hoshi, T. Iwamoto and H. Shinoda, "Non-contact tactile sensation synthesized by ultrasound transducers," in World Haptics 2009 - Third Joint EuroHaptics conference and Symposium on Haptic Interfaces for Virtual Environment and Teleoperator Systems, Salt Lake City, UT, USA, 2009, pp. 256-260.
21. T. Hoshi et al., "Noncontact Tactile Display Based on Radiation Pressure of Airborne Ultrasound," IEEE Transactions on Haptics, vol. 3, no. 3, pp. 155-165, Jul.-Sep. 2010.
22. T. Hoshi, "Development of Aerial-Input and Aerial-Haptic-Feedback System," in 2011 IEEE World Haptics Conference, Istanbul, Turkey, 2011, pp. 569-573.
23. K. Hasegawa and H. Shinoda. "Aerial Display of Vibrohaptic Sensation with High Spatial-Temporal Resolution Using Large-Aperture Airborne Ultrasound Phased Array," in IEEE World Haptics Conference, Daejeon, South Korea, 2013, pp. 31-36.
24. Y. Monnai et al., "HaptoMime: Mid-Air Haptic Interaction with A Floating Virtual Screen," in Proceedings of the 27th Annual ACM Symposium on User Interface Software and Technology, Honolulu, HI, USA, 2014, pp. 663-667.
25. S. Inoue, Y. Makino, and H. Shinoda, "Producing airborne ultrasonic 3D tactile image by time reversal field rendering," in 2014 Proceedings of the SICE Annual Conference (SICE), Sapporo, Japan, 2014, pp. 1360-1365.
26. K. Hasegawa, L. Qiu and H. Shinoda, "Midair Ultrasound Fragrance Rendering," IEEE Transactions on Visualization and Computer Graphics, vol. 24, no. 4, pp. 1477-1485, Apr. 2018.
27. L. R. Gavrilov, "The Possibility of Generating Focal Regions of Complex Configurations in Application to the Problems of Stimulation of Human Receptor Structures by Focused Ultrasound," Acoustical Physics, vol. 54, no. 2, pp. 269-278, Mar.-Apr. 2008.
28. T. Carter et al.,"UltraHaptics: Multi-Point Mid-Air Haptic Feedback for Touch Surfaces," in ACM Symposium on User Interface Software and Technology, St. Andrews, UK, 2013, pp. 505-514.
29. B. Long et al., " Rendering Volumetric Haptic Shapes in Mid-Air Using Ultrasound," ACM Transactions on Graphics, 2014, vol. 33, no.6, pp. 1-10, Nov. 2014.
30. G. Korres and M. Eid, "Haptogram: Ultrasonic Point-Cloud Tactile Stimulation," IEEE Access, vol. 4, pp. 7758-7769, 2016.
31. R. Roemer, W. Swindell, S. Clegg et al., "Simulation of focused, scanned ultrasonic heating of deep seated tumors, " IEEE Transactions on Sonics and Ultrasonics, vol. 31, no.5, pp. 457-466,1984.
32. X. Xin et al., "A Review of Smart Materials in Tactile Actuators for Information Delivery, " Journal of Carbon Research, vol. 3, no.4, pp. 38-50, Aug.-Dec. 2017.